X-ray Absorption Fine Structure of Ions Attracted by a Zwitterionic Surface Monolayer

Makoto Harada,[†] Tetsuo Okada,*[,†] and Iwao Watanabe[‡]

Department of Chemistry, Tokyo Institute of Technology, Meguro-ku, Tokyo 152-8551, Japan, and Department of Environmental Sciences, Osaka Women's University, Sakai, Osaka 590-0035, Japan

Received: June 6, 2002; In Final Form: December 11, 2002

The adsorption isotherms of Zn^{2+} and Br^- on a zwitterionic surface monolayer and their local structures have been studied by total-reflection total-conversion helium ion yield X-ray absorption fine structure (TRTCY-XAFS). The surface monolayer is prepared by spontaneous adsorption of *N*-dodecyl-*N*,*N*-dimethylammonio-butane sulfonic acid (DDABS) on an aqueous solution surface from a bulk solution. The adsorption of Zn^{2+} on the surface monolayer depends on the nature of coexistent anions; a poorly hydrated large anion such as ClO_4^- are well partitioned into the DDABS monolayer, and Zn^{2+} is attracted by generated negative potential. TRTCY-XAFS spectra indicate that Zn^{2+} attracted by the surface monolayer is mostly hydrated, but is partly bound by the sulfonic acid in DDABS, particularly when the large negative potential is induced by anion-partition. The TRTCY-XAFS spectra of Br^- also imply the coexistence of hydrated Br^- and that bound by the ammonium group in the surface monolayer. The calculation using FEFF, ver.7.02, suggests that the interaction distance between Br^- and water in the surface monolayer (3.15 Å) is shorter than that in bulk water (3.20 Å). In the surface monolayer, the availability of water molecules is limited, and thus the second coordination shell cannot be formed around Br^-. This weakens the interaction between water molecules, and results in the shorter coordination distance for Br^-.

Recent developments of methodologies and instruments have allowed us to study interfacial chemistry on molecular bases. The important involvements of interfacial phenomena have been confirmed in various aspects of biological, environmental, and industrial systems.[1] In particular, the interfaces involving liquid phases are of fundamental and practical importance, and have received much attention and interest. Spectroscopy, electrochemistry, and molecular simulation have indicated that the structures of molecules (including solvents) at an interface are different from those in bulk.[2] Although fluorescence and nonlinear spectroscopy have provided efficient information on the interfacial structures of some molecules, to which these methods are accessible, the structures of the targeted molecules are often complex and sometimes of less general interest.[2(a)−2(e)] In contrast, the solvation structures of simple ions at interfaces should be more important, because their behaviors are expected to play essential roles in various systems noted above. However, only very few approaches are available, which are sensitive and selective to simple ions present at interfaces.

X-ray absorption fine structure (XAFS) is a useful tool to probe the solvation structures of ions, and usually applied to structural analyses in condensed bulk phases. The authors developed a total-reflection total-conversion helium ion yield (TRTCY) XAFS, which is sensitive to ions present at air/solution interfaces.[3] In this method, the incidence X-ray is introduced on the solution surface at a grazing angle satisfying the total reflection condition at the energy of the X-ray. X-ray absorption occurs only within several tens of angstroms of the surface.[4] Generated photoelectrons and Auger electrons ionize He just above the solution. The ionization of He multiplicatively occurs, and detection sensitivity is greatly enhanced. The surface-selective and sensitive XAFS measurements are thus feasible. This method has some advantages over other spectroscopic methods: (1) high atom-selectivity, (2) applicability to most of the ions of general interest, (3) providing both structural and molar information at the interface, and (4) simultaneous access to both cationic and anionic information. When a charged surface monolayer is formed, oppositely charged ions are electrostatically attracted by the monolayer, and condensed in the electrical double layer. According to the electrostatic theory, the thickness of the electrical double layer is several tens of angstroms in a 10 mM solution of a 1:1 electrolyte, which corresponds to the detection depth of TRTCY-XAFS. This approach can thus visualize the events taking place within the electrical double layer of a charged surface monolayer.

In this paper, the surface structures and amounts of ions accumulated by a *N*-dodecyl-*N*,*N*-dimethyl-ammonio-butane-sulfonate (DDABS) surface monolayer are studied with TRTCY-XAFS.

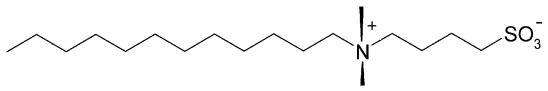

DDABS

DDABS is a zwitterionic surfactant having an inner cationic ammonium and outer anionic sulfonic group. Although both anions and cations can be attracted by this zwitterionic molecule, it is known that the character and concentration of anions govern the uptake of ions into zwitterionic micelles or surfaces.[5] Thus, negative surface potential is usually induced by anion-dominated partition. Our previous chromatographic[5(a)] and electrophoretic work[5(b)] have implied that large and poorly hydrated anions form

* Author to whom correspondence should be addressed. Phone and Fax: +81-3-5734-2612. E-mail: tokada@chem.titech.ac.jp.
[†] Tokyo Institute of Technology.
[‡] Osaka Women's University.

10.1021/jp026248n CCC: $25.00
Published on Web 02/15/2003

tight ion-associates with the ammonium groups in the zwitterionic molecule, whereas small and well-hydrated anions are still hydrated in the zwitterionic layer; perchlorate and chloride represent these two classes, respectively, and bromide is intermediate. Both cations and anions, which are attracted by the zwitterionic monolayer in different ways, can be simultaneously studied by TRTCY-XAFS; this is a significant advantage of this approach. We focus our attention on the solvation structure and surface concentration of Br^- and Zn^{2+} attracted by the DDABS monolayer, and get further insights into the molecular mechanisms in the ion uptake of zwitterionic layers.

Experimental Section

TRTCY-XAFS Method. The details of TRTCY-XAFS measurements were described in a previous paper.[3] The system used in this work was basically the same as used previously. X-ray radiation was introduced to an aqueous solution surface at a grazing angle; the critical angle of the total reflection at the Zn *K* edge (9.7 keV) is ca. 2.5 mrad, and that at the Br *K* edge (13.8 keV) is ca. 2.0 mrad. In this study, the incidence angles were set to ca. 1.1 mrad for Zn and 0.8 mrad for Br. The evanescent wave generated at the air/water interface by the irradiation of X-ray causes the ejection of photoelectrons and Auger electrons from the interfacial region to the upper atmosphere. The number of the ejected electrons is proportional to X-ray (evanescent wave) absorption. The cell was filled with He gas, which was ionized by the ejected electrons, especially by Auger electrons with high kinetic energy. Helium ions were collected by the cathode (placed 1 cm above the water surface), to which an appropriate bias voltage (150 V) was applied. X-ray absorption signals were amplified by a factor of ca. one thousand by this procedure. The incidence X-ray intensity was detected by a 4 cm ion-chamber filled with N_2 gas. As the TRTCY-XAFS measurement using this cell was highly surface-sensitive, the slight vibration of the surface severely interfered with the measurements. The cell floated on an ethylene glycol−water mixture to reduce effects of vibrations. All XAFS measurements were performed at BL-7C of Photon Factory, High Energy Accelerator Research Organization in Tsukuba, Japan.

Samples. Sample solutions, 3, 5, 10, 20, or 40 mM $ZnCl_2$, $ZnBr_2$, ZnI_2, or $Zn(ClO_4)_2$ containing 5 mM DDABS, were prepared with water purified by a MilliQ system. DDABS was synthesized by the reaction of dodecyl-dimethylamine with butanesultone, and purified by recrystallization. The zinc salts of special grade were purchased from KANTO Chemicals, and used as received.

Data Analysis. The normalized XAFS interference function, $\chi(k)$, is defined as

$$\chi(k) = \frac{\mu(k) - \mu_b(k) - \mu_0(k)}{\mu_0(k)} \quad (1)$$

$$k = \sqrt{\frac{2m}{\hbar^2}(E - E_0)} \quad (2)$$

where m is the electron mass, E is the incidence X-ray energy, E_0 is the threshold energy, and $\mu(k)$, $\mu_0(k)$, and $\mu_b(k)$ are the total absorption, the absorption due only to the K shell excitation of a priori isolated targeted atom, and the background absorption depending on the circumstances of the absorbing atom, such as absorption from the other shells and long-range solvation effects, respectively. The background absorption, $\mu_b(k)$, was determined by fitting the spectra at $E < E_0$ to Victoreen's formula, $aE^{-3} - bE^{-4} - c$; the Victoreen's parameters, a and b that are consistent with the literature values were selected.[6] The $\mu_0(k)$ was extracted in the same manner as reported previously.[7]

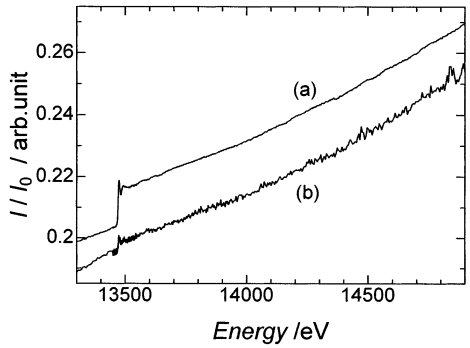

Figure 1. Comparison of TRTCY-XAFS edge jumps with and without DDABS surface monolayer. Subphase, 5 mM $ZnBr_2$ + 5 mM DDABS.

The XAFS spectra in k space, $\chi(k)$, were analyzed by curve-fitting with eqs 3 and 4:

$$\chi(k) = \sum_j \frac{S_j N_j F_j(k_j)}{k r_j^2} \exp(-2\sigma_j^2 k_j^2) \sin[2k_j r_j + \phi_j(k_j)] \quad (3)$$

$$k_j = \sqrt{k^2 - \frac{2m}{\hbar^2}\Delta E_{0j}} \quad (4)$$

where j is the coordination shell number, r_j is the distance between the absorbing atom and a scattering atom, S_jN_j is the amplitude factor (where S_j is the amplitude reduction factor), σ_j is the Debye−Waller factor), E_{0j} is the absorption edge shift, and $F_j(k_j)$ is the backscattering amplitude. The factors $\phi_j(k_j)$ and $F_j(k_j)$ were calculated with FEFF, ver. 7.02. In this work, XAFS parameters were determined by curve-fitting using phenomenological models.

Results and Discussion

Edge Jump. Figure 1 compares the TRTCY-XAFS spectra for 10 mM Br^- aqueous solution at Br *K*edge with and without the DDABS surface monolayer. The edge jump obtained in the presence of the surface monolayer is much larger than that without the monolayer, indicating Br^- attracted by the DDABS monolayer is condensed near the surface. The small edge jump seen even in the absence of the DDABS surface monolayer comes from Br^- present just below the solution surface. The detection depth of the present method was calculated as ca. 100 Å, though it is varied with the angle and energy of incidence X-ray. As the detection area on the solution surface was ca. 10 mm × 50 mm, the detection volume below the surface is ca. 5 nL, which contains 50 pmol Br^- for 10 mM solution. Assuming that a DDABS molecule occupies 1.3 nm^2 of the surface area (this value was calculated from the micellar size and aggregation number for dodecyldimethylammonio propanesulfonic acid, DDAPS[8]), ca. 0.6 nmol of DDABS molecules are present in the detection area; the actual surface density of DDABS must be larger. The surface concentration of DDABS is equal to the maximum surface concentration of Br^- if it is bound by DDABS with 1:1 stoichiometry. Thus, it is possible that the DDABS surface monolayer enhances the TRTCY-XAFS signal by a factor of ca. 10. Similar discussions hold for cations if an appropriate stoichiometry is taken into consideration.

The edge jump amplitudes should be proportional to the number of the absorbing atoms within the detection volume, meaning that the adsorption isotherms for ions on the surface

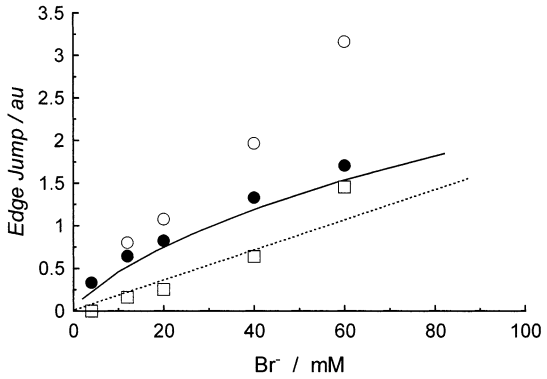

Figure 2. Adsorption isotherm of Br^-. Subphase: $CuBr_2$. Open circles, edge jump measured with DDABS surface monolayer; squares, edge jumps measured without DDABS surface monolayer; solid circles, net edge jump of Br^- attracted by the DDABS monolayer. Solid curve shows the result of calculation with parameters $K_{ani} = 10^{-2}$ M^{-1}, $K_{cat} = 2 \times 10^{-2}$ M^{-1}, $\lambda = 100$ Å, and $d = 5$ Å.

monolayer can be obtained by measuring the edge jump.[3] Figure 2 shows a relation between the edge jump amplitudes and concentration of Br^- in the subphase. In the absence of the surface monolayer, the amount of Br^- in the detection volume linearly increases with increasing concentration of Br^- in bulk solutions (shown by open squares in the figure). The adsorption of DDABS on the surface enhances edge jumps to a significant extent. Since the measured edge jump thus comes not only from Br^- accumulated by the surface monolayer but also from that in the subphase, the latter contribution should be subtracted from a measured edge jump. Solid circles in Figure 2 show the values after correcting the contribution from the bulk Br^-; this curve can reasonably be regarded as an adsorption isotherm of Br^- on the surface DDABS monolayer. In the usual ex situ experiments, adsorbed molecules must be considered as species fixed on the surface of adsorbents. As discussed in details below, the adsorbed species detected by the present method include ions accumulated in the diffuse layer as well as those tightly bound by the surface monolayer. Although Zn^{2+} and Cu^{2+} were examined as countercations, no difference in Br^- adsorption was detected.

The adsorption of cations strongly depends on the nature of anions unlike that of Br^-. Figure 3 shows the dependence of the edge jump at the Zn *K* edge on the concentration of $ZnCl_2$, $ZnBr_2$, ZnI_2, or $Zn(ClO_4)_2$ in the presence of the DDABS surface monolayer. The contribution from bulk Zn^{2+} was subtracted from the measured edge jump. The surface concentrations of Zn^{2+} increase in the order of $ZnCl_2 < ZnBr_2 < ZnI_2 < Zn(ClO_4)_2$, indicating that ClO_4^- most strongly interacts with the DDABS monolayer, and Zn^{2+} is attracted by the negative potential induced by anion-partition into the monolayer. This agrees with previous observations with different approaches.[5] The reasons that anion properties dominate overall ion partition into the DDABS layer are 2-fold. One is the structural reason of the DDABS molecule, in which the cationic group is located inside whereas the anionic group is outside. This induces the strong positive electrostatic potential field in the dipolar layer. Although cations are attracted by the negative potential induced by anion partition and reduce the inner positive potential (also outer negative potential) to some extent, the potential reduction by cation interaction is marginal for identically charged cations. Another reason is a difference in the hydration nature of ions. Anions studied in this work are much more weakly hydrated than divalent cations such as Cu^{2+} and Zn^{2+}. The partition of ions into the zwitterionic layer should be accompanied by

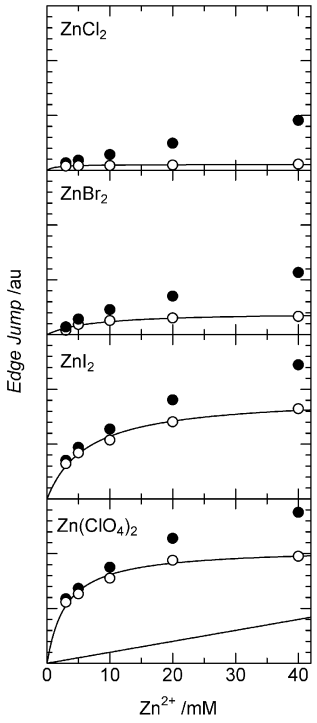

Figure 3. Adsorption of Zn^{2+} on the surface monolayer of DDABS from various zinc salt solutions. Solid circles, TRTCY-XAFS edge jump. Open circles, after correction of a signal from bulk solution. The solid line shown in the $Zn(ClO_4)_2$ box represents the edge jump signal from bulk Zn^{2+}. Solid curves are the results of calculations with parameters $K_{ani} = 0$ (Cl^-), 10^{-2} M^{-1}(Br^-), 0.5 M^{-1}(I^-), and 0.9 M^{-1}(ClO_4^-), $\Delta G_i^\circ = 800$ J mol^{-1} for Cl^-, $K_{cat} = 2 \times 10^{-2}$ M^{-1}, $\lambda = 100$ Å, and $d = 5$ Å.

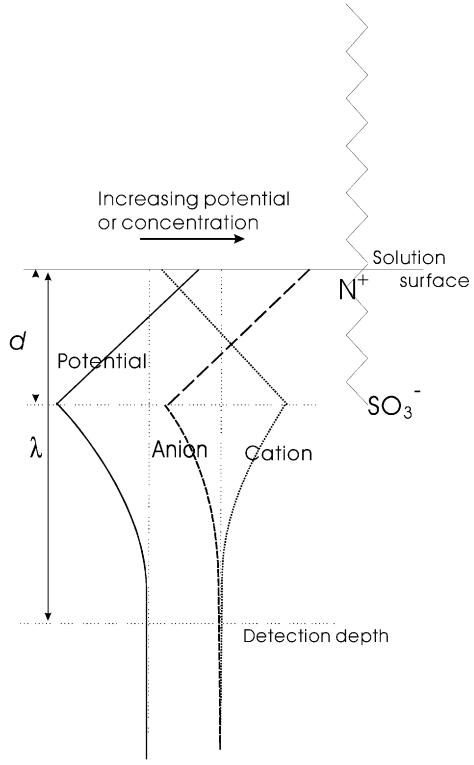

Figure 4. Schematic representation of electrostatic potential and ionic distributions in the vicinity of DDABS surface monolayer.

complete (or partial) dehydration of the ions. Weakly hydrated anions should thus be more well-partitioned than strongly hydrated cations.

The ζ-potential of *N*-dodecyl-*N*,*N*-dimethyl-ammonio-propanesulfonate (DDAPS) micelles and chromatographic retention of anions on the DDAPS-modified stationary phase were successfully interpreted on the basis of the model derived from the Poisson−Boltzmann theory.[5(a)] It is known that the Poisson−Boltzmann theory does not give a good approximation for multivalent electrolytes. Keeping this limitation in mind, we attempted to apply this model to the present results. Two mechanisms were assumed to explain the partition (adsorption) selectivity: (1) ions form ion-associates with the ionic groups of DDABS molecules, and (2) ions undergo the solvation changes inside the layer (basically the layer between the ammonium and sulfonic acid groups, hereinafter this layer is called the dipolar layer). Figure 4 schematically shows the profiles of electrostatic potential and ionic concentrations in the electrical double layer of the DDABS monolayer. When no ion-associates are formed, ionic distributions are described by the Boltzmann theory as shown by solid curves. Since the evanescent wave intensity decreases with increasing distance from the surface in an exponential fashion,[4] the detection sensitivity is varied with the depth of the layer where X-ray absorbing ion is located. Thus, the TRTCY-XAFS signals originating from a solute not forming an ion-associate are given by

$$S_{\text{dipole}} = n_i \int_0^d \left\{ \exp\left(- \frac{z_i \psi_{\text{dipole}}(x) - \Delta G_i^\circ}{RT} \right) - 1 \right\} \exp\left(- \frac{x}{\lambda} \right) \mathrm{d}x \quad (5)$$

$$S_{\text{out}} = n_i \int_d^\lambda \left\{ \exp\left(- \frac{z_i \psi_{\text{out}}(x)}{RT} \right) - 1 \right\} \exp\left(- \frac{x}{\lambda} \right) \mathrm{d}x \quad (6)$$

where S_{dipole} and S_{out} are the signals coming from an ion of interest present in the dipolar layer and outside of the monolayer, $\psi_{\text{dipole}}(x)$ and $\psi_{\text{out}}(x)$ are the electrostatic potential in the dipolar layer and outside of the monolayer, n_i and z_i are the bulk concentration and charge of the analyte ion, ΔG_i° is the Gibbs free energy of transfer from the bulk to the dipolar layer, d is the thickness of the dipolar layer, and λ is the specific penetration depth of the evanescent wave under a given experimental condition. The first parentheses in the integrals of these equations represent the excess amount of the ion, and the second represents the evanescent wave intensity at x. It is reasonably assumed that an analyte ion undergoes a solvation change only in the dipolar layer, and thus ΔG_i° is included in eq 5 but not in eq 6.

When an ion forms an ion-associate at a specific distance, the signals coming from the ion-associate are given by the follow equations:

$$S_{\text{ia(anion)}} = \frac{s K_{\text{ani}} n_i \exp\left(- \dfrac{z_i \psi_1 - \Delta G_i^\circ}{RT} \right)}{1 + K_{\text{ani}} n_i \exp\left(- \dfrac{z_i \psi_1 - \Delta G_i^\circ}{RT} \right)} \exp\left(- \frac{r_1}{\lambda} \right) \quad (7)$$

$$S_{\text{ia(cation)}} = \frac{s K_{\text{cat}} n_i \exp\left(- \dfrac{z_i \psi_2}{RT} \right)}{1 + K_{\text{cat}} n_i \exp\left(- \dfrac{z_i \psi_2}{RT} \right)} \exp\left(- \frac{r_2}{\lambda} \right) \quad (8)$$

where $S_{\text{ia(anion)}}$ and $S_{\text{ia(cation)}}$ are the signals for an anion and a cation, K_{ani} and K_{cat} are the ion-association constants for an anion and cation, s is the surface concentration of DDABS, r_1 and r_2 are the distances between the surface and the ammonium group or the sulfonic acid group, respectively, and ψ_1 and ψ_2 are the electrostatic potential at r_1 and r_2, respectively. The ion-association of a cation occurs at the outer surface of the surface monolayer, and thus ΔG_i° is not included in eq 8. The molecular modeling indicates that the distance between the ammonium nitrogen and the sulfonic sulfur in the DDABS molecule is 5 Å; thus $r_2 - r_1 = 5$ Å. If the reflection of X-ray occurs at the water surface, r_1 should be nearly zero. In contrast, if the reflection occurs at the hydrocarbon end of the DDABS molecule, r_1 must be equal to ca. 19 Å according to molecular modeling. The calculations were carried out with these two different parameters. Thus, the total signal intensity, which is comparable with an experimental adsorption isotherm, is equal to $S_{\text{dipole}} + S_{\text{out}} + S_{\text{ia(anion or cation)}}$.

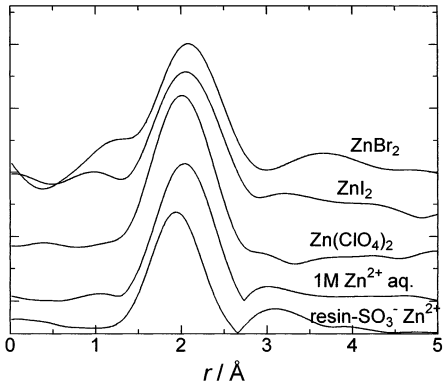

Figure 5. Fourier transforms of TRTCY-XAFS spectra for Zn^{2+} attracted by the DDABS surface monolayer. For comparison, the Fourier transforms of the transmission XAFS spectra of Zn^{2+} in bulk water and that in a dry sulfonate-type cation-exchange resin are also illustrated.

Fitting curves in Figures 2 and 3 show the results of calculation with the above equations, where r_1 was assumed zero because better fittings were possible. Since it is difficult to directly compare the adsorption isotherms with calculated signal intensities because of a difference in dimensions, calculated values were multiplied by an appropriate coefficient to make comparison easier. Ion-associate formation was assumed a primary mechanism because it gave better fittings than the assumption of different hydration; this will prove appropriate from the structural analyses, vide infra. The following parameters were suitable for explanation of the adsorption isotherms for both Br^- and Zn^{2+}; $K_{\text{ani}} = 10^{-2}$ $M^{-1}(Br^-)$, 0.5 $M^{-1}(I^-)$, 0.9 $M^{-1}(ClO_4^-)$, and $K_{\text{cat}} = 2 \times 10^{-2}$ M^{-1}. $K_{\text{ani}} = 0$ and weaker hydration in the monolayer than in bulk by $\Delta G_i^\circ = 800$ J mol^{-1} should be assumed for Cl^-. Although ion association constants for anions are slightly smaller than those determined for DDAPS, basic trends are identical.[5(a)−(c)] The anion-governing partition mechanism is thus confirmed for the zwitterionic surface monolayer.

Structure of Zn^{2+} at the Solution Surface. Figure 5 shows the Fourier transforms of the TRTCY-XAFS spectra at the Zn *K* edge for 20 mM $ZnBr_2$, ZnI_2, and $Zn(ClO_4)_2$ aqueous solutions with 5 mM DDABS. The Fourier transforms for 1 M Zn^{2+} aqueous solution and for Zn^{2+} in a dry sulfonate-type cation-exchange resin are also shown for comparison; the XAFS spectra for these were obtained by a usual transmission mode. These Fourier transforms were calculated in the range $k = 3.2-10$ $Å^{-1}$ with the parameters determined by FEFF, ver.7.02. This figure indicates that there is a difference in the coordination distance between $r_{\text{Zn−O(water)}}$ = ca. 2.1 Å and $r_{\text{Zn−O(−SO}_3\text{−)}}$ = ca. 1.95 Å. The main peak positions for surface Zn^{2+} are between, indicating that both hydrated and bound Zn^{2+} contribute to the spectra. Although these two contributions were not separated, qualitative interpretation is possible. The spectra

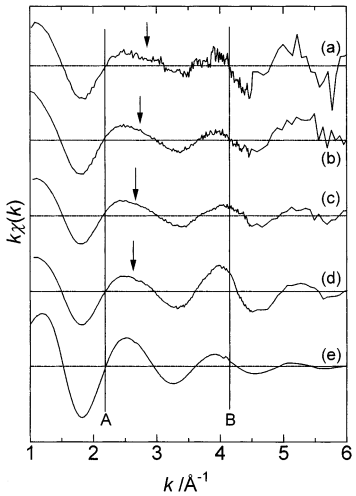

Figure 6. $\chi(k)k$ spectra for Br^- attracted by the DDABS surface monolayer from (a) 5 mM, (b) 10 mM, (c) 20 mM, and (d) 40 mM $ZnBr_2$, and (e) Br^- in bulk water. Arrows point at shoulders, which suggest the presence of Br^- bound by an ion-exchange group.

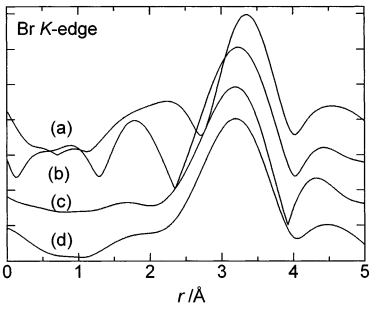

Figure 7. Fourier transforms of TRTCY-XAFS spectra of Br^- attracted on the DDABS surface monolayer. (a) 5 mM, (b) 10 mM, (c) 20 mM, and (d) 40 mM $ZnBr_2$.

involve the contributions both from Zn^{2+} in bulk and from that accumulated in the surface monolayer. The ratio of the former contribution to the overall signal intensity can be estimated from the adsorption data shown in Figure 3. The contribution from hydrated Zn^{2+} present in bulk occupies 57%, 23%, and 13% for 20 mM $ZnBr_2$, ZnI_2, and $Zn(ClO_4)_2$ subphase, respectively. This means that the XAFS spectrum obtained with 20 mM $ZnBr_2$ is composed of 57% of the spectra of hydrated Zn^{2+} and 43% of that of Zn^{2+} accumulated by the surface monolayer, and the latter becomes dominant in the order of $ZnBr_2 < ZnI_2 < Zn(ClO_4)_2$. Thus, the TRTCY-XAFS for $ZnBr_2$ is most strongly affected by $r_{Zn-O(water)}$; actually, the peak position is almost the same as that of Zn^{2+} in aqueous solution. The main peak position approaches that for $r_{Zn-O(-SO_3-)}$ in the dry resin in the order of $ZnBr_2$, ZnI_2, and $Zn(ClO_4)_2$; this trend correlates well with the order of decreasing the relative contribution from hydrated Zn^{2+} present in subphases. A shift of the peak position to smaller r suggests that Zn^{2+} attracted by the DDABS surface monolayer is bound by the sulfonic acid group to some extent, particularly when highly negative potential is induced by the partition of anions into the monolayer; ClO_4^- is just the case. Although detailed analyses were attempted, clear conclusions have not been drawn because TRTCY-XAFS spectra were rather noisy.

Structure of Br^- at the Solution Surface. Figures 6 and 7 show the $\chi(k)k$ spectra and Fourier transforms derived from the TRTCY-XAFS spectra for Br^-. Fourier transforms were carried out over the range $k = 1-6$ Å^{-1}. The oscillation periods for (c) and (d) are longer than those for (a) and (b), clearly

TABLE 1: XAFS Parameters Determined for Br^- Attracted by the DDABS Surface Monolayer[a]

concentrated Br^- in subphase/mM	r/Å	N[b]	σ/Å
(a) 10	3.41	3.47	0.152
(b) 20	3.42	3.88	0.152
(c) 40	3.20	3.03	0.107
(d) 80	3.18	5.24	0.096
Br^- in bulk[c]	3.20	6.00	0.144

[a] Oxygen was assumed a scattering partner. [b] The coordination number in bulk water was assumed 6. [c] Determined by transmission XAFS for 3M KBr aqueous solution.

suggesting that the longer interaction distance be included in the latter cases. The results of curve fitting are summarized in Table 1. It should be noted that the distance between Br^- and scattering atoms becomes short as the concentration of Br^- increases. The $r_{Br-O(water)}$ is 3.20 Å in a bulk solution, which is equal to r determined for (c) and (d), while r for (a) and (b) is obviously longer. We previously examined the solvation structure of Br^- in anion-exchange resins, and revealed that the interaction distance between Br^- and the trimethylammonium group in the resin was 3.4−3.5 Å,[6(b)] which is almost equal to the coordination distance of Br^- in aprotic solvents;[9] this should be characteristic of the weak interaction of Br^-. It is thus reasonable to consider that the interaction distance for Br^- bound by the ammonium ion in the DDABS monolayer should be ca. 3.5 Å. The contribution from Br^- present in a subphase to the TRTCY-XAFS signal becomes more dominant in higher concentrations of Br^-; this contribution is more than 50% in 40 and 80 mM Br^- as shown in Figure 2. Since Br^- accumulated by the surface monolayer is in part still hydrated (see the discussions below), Br^- bound by the ammonium group occupies only a minor portion of detectable Br^- for (c) and (d). In contrast, Br^- dominantly exists in the dipolar layer for 10 and 20 mM Br^-, and effects of subphases are marginal. Thus, the relative amount of Br^- bound by the ammonium group becomes large for diluted subphases. This results in the longer interaction distance for (a) and (b). The fittings were carried out with Br−O parameters for all the spectra. If the bound Br^- becomes dominant, use of Br−O parameters involves inconsistency. Since the spectra are basically the superimposition of two different ones, coming from Br−O and Br−C (or N), precise analyses are impossible by assuming a single scattering partner. The detailed analyses are shown below, in which two different scattering atoms are taken into account.

The $\chi(k)k$ spectra shown in Figure 6 suggest another interesting feature of Br^- attracted by the DDABS surface monolayer. All of these spectra have clear shoulders at $k = 2.5-3$ Å^{-1} and oscillation periods are obviously changed, indicating that they involve more than two different structures. As discussed above, both the surface ion-associates and hydrated Br^- present in a subphase contribute to TRTCY-XAFS spectra. It is thus natural that the $\chi(k)k$ spectra (c) and (d) involve two different structures, because these involve ca. 50% contribution from Br^- in the subphases; hydrated Br^- is dominantly detected under these conditions. In contrast, the contribution from hydrated Br^- in a subphase is marginal for relatively diluted subphases (a) and (b). It should be noted that, despite this fact, the $\chi(k)k$ spectra (a) and (b) indicate the presence of not less than two species. There are two possible explanations for this feature: (1) Br^- forming the ion-associate is still hydrated, and (2) there coexist the ion-associate of Br^- and hydrated Br^- in the dipolar layer. The coordination number of surface Br^- for (a) and (b) is 3−4 as listed in Table 1. If Br^- simultaneously interacted with the ammonium group in the DDABS molecule and water ligands,

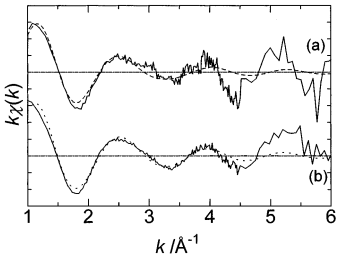

Figure 8. $\chi(k)k$ spectra for Br^- attracted by the DDABS surface monolayer from (a) 10 mM and (b) 20 mM, and results of calculation (broken curves) assuming the coexistence of hydrated Br^- and bound Br^-. Details are given in the text.

this number would be larger. Hence, the results of XAFS analysis imply the coexistence of Br^- bound by the ammonium ion and hydrated one in the dipolar layer of the DDABS monolayer.

It was attempted to reproduce $\chi(k)k$ spectra (a) and (b) by superimposing two different spectra originating from Br−C (ion-associate) and Br−O (hydrated); the calculation was based on FEFF, ver.7.02. In the ion-associate, both the methyl carbons and the ammonium nitrogen can be scattering partners. Since molecular modeling indicated that the Br−N distance is longer than Br−C in any geometry, Br−C rather than Br−N is taken into consideration. When the interaction distances were assumed 3.5 Å (Br−C) and 3.2 Å (Br−O), $\chi(k)k$ spectra (a) and (b) could not be reproduced. The shorter interaction (3.15 Å) distance for Br−O has finally proven suitable to explain the $\chi(k)k$ spectra (a) and (b) as shown in Figure 8. The broken curves are given by the following relations:

$$\chi(k)k = 6.4\chi_{Br-C}(k)k + 3.8\chi_{Br-O}(k)k \quad \text{(for Figure 8a)}$$

$$\chi(k)k = 6.4\chi_{Br-C}(k)k + 4.8\chi_{Br-O}(k)k \quad \text{(for Figure 8b)}$$

These calculated spectra agree with experimental ones except for high k range (>4.5 Å). The coefficients in the above equations indicate that the amount of ion-associate is not changed, but that of the hydrated one increases with increasing bulk Br^- concentration from 10 to 20 mM. The shorter Br−O distance in the dipolar layer than that in bulk water can be interpreted by taking the hydration environment in the dipolar layer into consideration. In the bulk water, coordinated water ligands interact with water molecules surrounding the coordination shell of Br^- by hydrogen bonding; this situation determines the Br−O distance (3.2 Å) in bulk water. In contrast, there exist few water molecules in the dipolar layer, and thus the interaction between a coordinating water molecule and that not participating in the coordination to Br^- should be weaker than in bulk where more water molecules are available. This results in stronger coordination and shorter coordination distance in the dipolar layer.

Conclusion

TRTCY-XAFS has been applied to Zn^{2+} and Br^- attracted by the DDABS surface monolayer. The condensation of Zn^{2+} strongly depended on the nature of coexistent anions, and was explained by the electrostatic calculation proposed in previous papers.[5(a)−(c)] The binding of Zn^{2+} by the monolayer was detected only when the high negative potential was induced at the outer surface of the monolayer due to the partition of anions. In contrast, Br^- directly bound by the ammonium groups in the DDABS monolayer was detected in any cases. The hydration structure of Br^- in the DDABS layer was different from that in bulk water; shorter coordination distance was implied. Thus, the present study has elucidated interesting features for ions partitioned into the zwitterionic layer. It is an advantage of the present approach over usual thermodynamic measurements that it provides not only the adsorption amounts of ions but also structural information. To our knowledge, we presented the first experimental evidence that the coordination distance of ions is changed in the vicinity of the charged surface. The present approach should be applied to different systems to verify the generality of this aspect.

Acknowledgment. This work was performed under the approval of Photon Factory Advisory Committee (Proposal Nos. 98G311 and 2001G113). The authors are grateful for the financial support by the REIMEI from the Japan Atomic Energy Research Institute and by the Sumitomo foundation.

References and Notes

(1) (a) Howe, J. M. Interfaces in materials: atomic structure, thermodynamics and kinetics of solid-vapor, solid−liquid and solid−solid; Wiley: New York, 1997. (b) Myers, D. Surfaces, interfaces, and colloids: principles and applications; VCH Publishers: New York, 1991

(2) (a) Naujok, R. R.; Paul, H. J.; Corn, R. M. *J. Phys. Chem.* **1996**, *100*, 10498. (b) Conboy, J. C.; Richmond, G. L. *J. Phys. Chem. B* **1997**, *101*, 983. (c) Gragson, D. E.; Richmond, G. L. *Langmuir* **1997**, *13*, 4804. (d) Benderskii, A. V.; Eisenthal, K. B. *J. Phys. Chem. B* **2000**, *104*, 11723. (e) Slyadnev, M. N.; Inoue, T.; Harata, A.; Ogawa, T. *Colloids Surf. A* **2000**, 164, 155. (f) Benjamin, I. *Chem. Rev.* **1996**, *96*, 1449. (g) Kim, J. S.; Lee, S. B.; Kang, Y. S.; Park, S. M.; Majda, M.; Park, J.-B. *J. Phys. Chem. B* **1998**, *102*, 5794. (h) Walker, R. A.; Gragson, D. E.; Richmond. G. L. *Colloids Surf. A* **1999**, *154*, 175. (i) Kitamura, F.; Nanbu, N.; Ohsaka, T.; Tokuda, K. *J. Electroanal. Chem.* **1998**, *452*, 241. (j) Wu, K.; Iedema, M. J.; Schenter, G. K.; Cowin, J. P. *J. Phys. Chem. B* **2001**, *105*, 2483. (k) Israelachvili, J. N.; Wennerström, M. *Nature* **1997**, *385*, 689. (l) Pemberton, J. E.; Joa, S. L.; Shen, A.; Kimball, J. W. *J. Chem. Soc. Faraday Trans.* **1996**, *92*, 3683. (m) Toney, M. F.; Howard, J. N.; Richer, J.; Borges, G. L.; Gordon, J. G.; Melroy, O. R.; Wiesler, D. G.; Yee, D.; Sorensen, L. B. *Nature* **1994**, *368*, 444. (n) Dang, L. X. *J. Phys. Chem. B* **1999**, *103*, 8195. (o) Michael, D.; Abenjamin, I. *J. Chem. Phys.* **2001**, *114*, 2817. (p) Si, S. K.; Gewirth, A. A. *J. Phys. Chem. B* **2000**, *104*, 10775. (q) Singh, P. K.; Adler, J. J.; Rabinovich, Y. I.; Moudgil, B. M. *Langmuir* **2001**, *17*, 468. (r) Schurhammer, R.; Wipff, G. *New J. Chem.* **1999**, *23*, 381. (s) Clavez, E. Le; Blaudez, D.; Buffeteau, T.; Desbat, B. *Langmuir* **2001**, *17*, 670.

(3) Watanabe, I.; Tanida, H.; Kawauchi, S.; Harada, M.; Nomura, M. *Rev. Sci. Instrum.* **1997**, *68*, 3307.

(4) (a) Parratt, L. G. *Phys. Rev.* **1954**, 95, 359. (b) Kawai, J.; Takami, M.; Fujinami, M.; Hashiguchi, Y.; Hayakawa, S.; Gohshi, Y. *Spectrochim. Acta B* **1992**, *47*, 983.

(5) (a) Okada, T.; Patil, J. M. *Langmuir* **1998**, *14*, 6241. (b) Iso, K.; Okada, T. *Langmuir* **2000**, *16*, 9199. (c) Masudo, T.; Okada, T. *Phys. Chem. Chem. Phys.* **1999**, *1*, 3577. (d) Kamenka, N.; Chorro, M.; Chevalier, Y.; Levy, H.; Zana, R. *Langmuir* **1995**, *11*, 4234. (e) da Silva, M.; Cuccovia, I.; Chaimovich, H.; Politi, M. J.; Reed, W. R. *J. Phys. Chem.* **1992**, *96*, 6442. (f) Bongiovanni, R.; Ottewill, R. H.; Rennie, A. R.; Laughlin, R. G. *Langmuir* **1996**, *12*, 4681.

(6) (a) Teo, B. K. EXAFS: Basic Principles and Data Analysis; Springer-Verlag: Berlin, 1985. (b) Lonsdale, K. International Table for X-ray Crystallography; Kynoch: Birmingham, 1968; Vol. 3.

(7) (a) Harada, M.; Okada, T. *Anal. Sci.* **2001**, *17*, 233. (b) Harada, M.; Okada, T.; Watanabe, I. *J. Phys. Chem. B* **2002**, *106*, 34.

(8) Chevalier, Y.; Kamenka, N.; Chorro, M.; Zana, R. *Langmuir* **1996**, *12*, 3225.

(9) Tanida, H.; Sakane, H.; Watanabe, I. *J. Chem. Soc. Dalton Trans.* **1994**, 2321.